

Supplementary information

## Microstructure and rheology of microfibril-polymer networks

Sandra J. Veen<sup>†\*</sup>, Peter Versluis<sup>†</sup>, Anke Kuijk<sup>†</sup> and Krassimir P. Velikov<sup>†‡\*</sup>

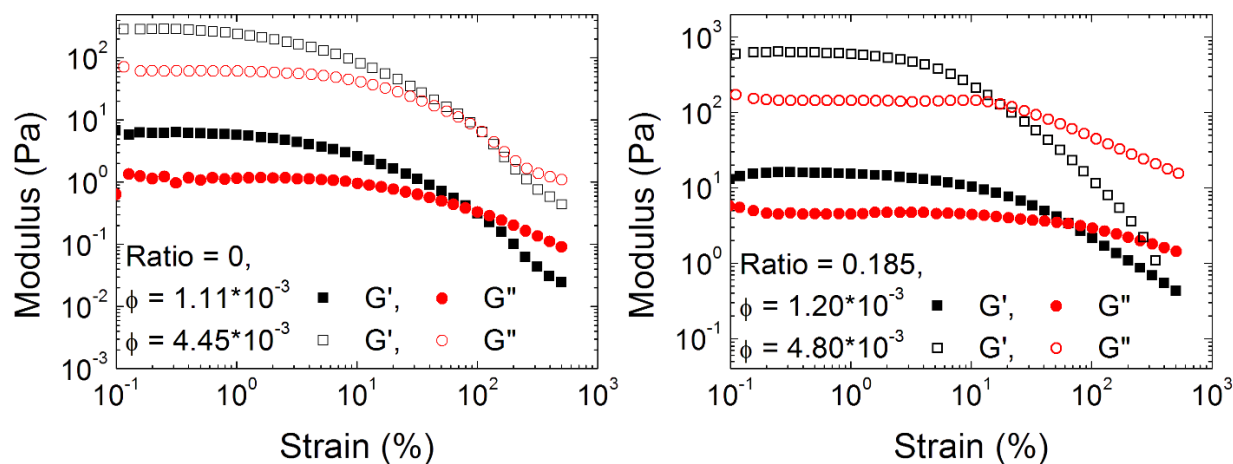
<sup>†</sup>Unilever Research Vlaardingen, Olivier van Noortlaan 120, 3133 AT Vlaardingen, The Netherlands

<sup>‡</sup>Soft Condensed Matter, Debye Institute for Nanomaterials Science, Department of Physics and Astronomy, Utrecht University, Princetonplein 1, 3584 CC Utrecht, The Netherlands

### S.I.1 Strain Sweeps of selected samples

In order to illustrate that the presented results in the manuscript are obtained in the linear viscoelastic regime, strain sweeps of representative samples are given in the figure below. Data is presented for both pure bacterial cellulose as well as for a CMC/BC ratio of 0.185. Curves are given for the lowest and highest BC concentrations used in experiments. The presented strain sweeps were performed at a frequency of 1 Hz. As can be seen, the chosen strain of 0.1% for the determination of the elastic and loss moduli is well within the linear strain regime.

The frequency sweeps were also performed at a strain of 0.1%. According to literature, the linear viscoelastic range (with respect to strain amplitude) shows little to no dependence on frequency, especially at frequencies  $\leq 10$  rad/sec. Deviation can be expected when the frequency sweep itself shows a large dependence of  $G'$  on frequency and/or a cross over from a  $G' > G''$  to a  $G'' > G'$  regime.<sup>1</sup> This is however, not observed for the microfibril systems. The presented strain sweeps shows deviation from the linear regime at strains an order of magnitude higher than the applied 0.1% and hence it is believed that the chosen strain is sufficient to remain in the linear regime throughout the frequency sweep.



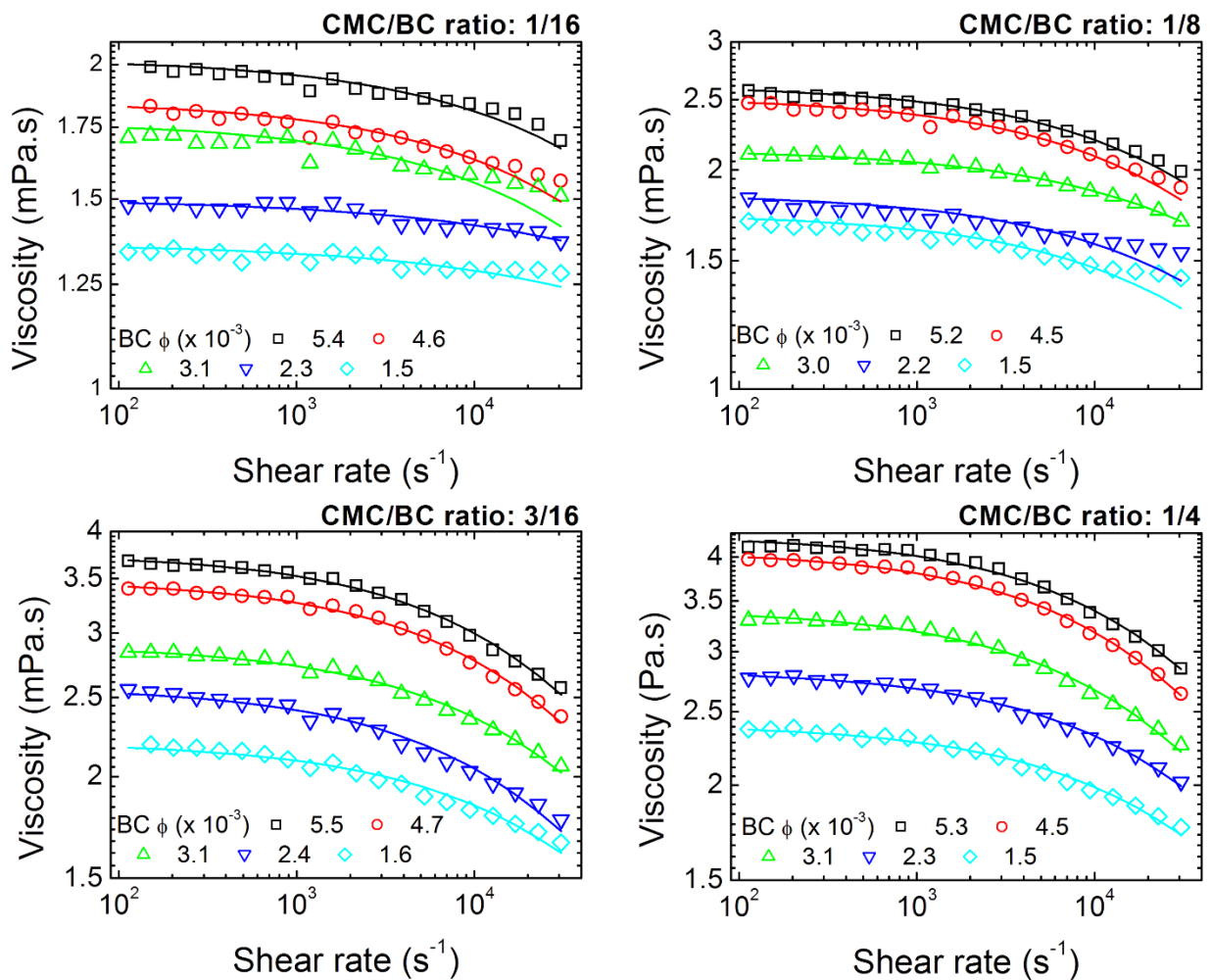
**Supporting Figure 1:** Strain sweep of BC suspensions at two different CMC/BC ratios and two BC concentrations (in volume fraction ( $\phi$ )).

## S.I.2 Viscosity measurements of the supernatants

After centrifugation to remove the bacterial cellulose (BC) microfibrils from the carboxymethyl cellulose (CMC) / BC mixtures, the viscosity as a function of shear rate of the obtained supernatants was fitted to a Cross/Williamson model<sup>2</sup>:

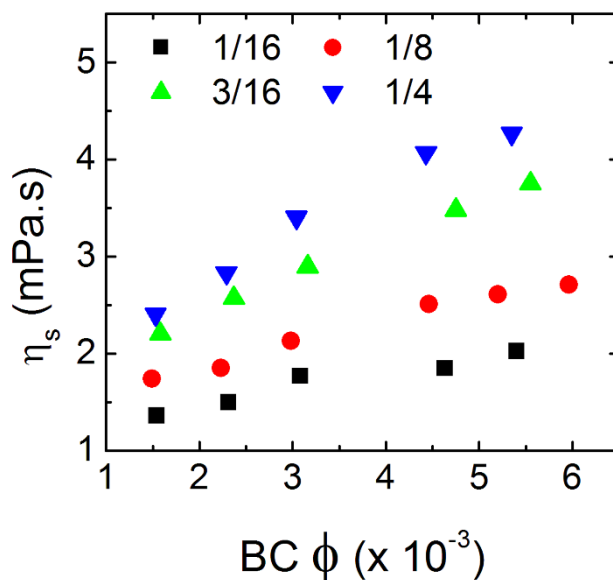
$$\eta = \frac{\eta_0}{1 + k\dot{\gamma}^p}$$

This is a well-known model for shear thinning fluids in which  $\eta$  is the measured viscosity,  $\dot{\gamma}$  the shear rate and  $k$  and  $p$  are constants.  $\eta_0$  is the first Newtonian plateau viscosity or zero shear viscosity which is dependent on the concentration of carboxymethyl cellulose present in the supernatant. The results of all the viscosity measurements and their fits are given in the graphs below.



**Supporting Figure 2:** Viscosity as a function of shear rate at different bacterial cellulose concentrations for supernatants obtained from different CMC/BC ratios and original BC concentrations (in volume fraction  $\phi$ ).

The results in Supporting Figure 2 show that the viscosity of the continuous phase depends not only on the starting CMC/BC ratio but also on the dilution made afterwards to obtain the series with different BC concentrations.



**Supporting Figure 3:** Zero shear viscosity of the supernatant/continuous phase for the different CMC/BC ratios as a function of BC concentration in volume fraction ( $\phi$ ).

### S.I.3 Estimated amount of CMC per BC microfibril surface area

To be able to place the results presented in the main article in a broader perspective the different CMC/BC weight ratios are converted to weight of CMC per surface area of BC microfibril. The microfibrils are known to be polydisperse and hence only an estimate can be made for the total surface area of the particles. It is not possible to give an estimate of the number of moles of CMC per BC surface area. The molecular weight of the CMC initially added to the suspensions changes due to the applied high energy de-agglomeration. It is known that high energy mechanical treatment can break polymers into smaller pieces<sup>3</sup>. For the presented system, the molecular weight for the CMC after Microfluidizer treatment is not known and hence no calculation for the number of moles can be performed.

As an approximation, the weight of CMC in mg per unit surface area of BC in  $m^2$  is given in the following table. This surface area is calculated by assuming a length of 15  $\mu m$ , width of 60 nm, height of 9 nm and BC density of 1.5  $gr/mL$ .<sup>4</sup> It has to be emphasize that not all CMC is adsorbed onto the

surface of the BC microfibrils and the numbers given represent the added CMC.

**Table 1:** Estimate of the amount of carboxymethyl cellulose added in mg per surface area of BC microfibril.

CMC/BC wt/wt	CMC/BC mg/m <sup>2</sup>
0.000	0.00
0.023	0.14
0.045	0.26
0.065	0.38
0.071	0.42
0.088	0.52
0.108	0.63
0.111	0.65
0.139	0.81
0.163	0.96
0.182	1.07
0.185	1.09
0.250	1.47

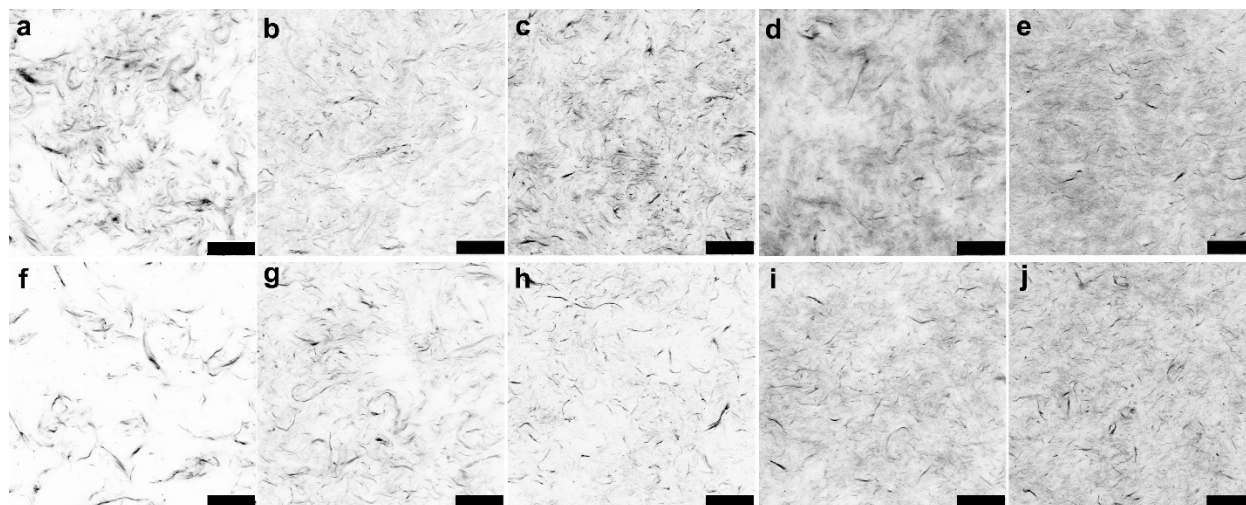
### S.I.4 Confocal image analysis

Images were taken at 40 times magnification. After converting to 8 bit, the confocal images without the scale bar were normalized by using the Enhance Contrast normalization option with 0.4% saturated pixels. From the resulting intensity histogram the full width at half maximum was determined and divided by 256 (number of grey values) to yield a number between 0 and 1.

The orientation of the microfibrils was determined with help of the OrientationJ plugin.<sup>5</sup> OrientationJ computes the orientation, energy and coherency maps of an image and its weighted orientation histogram. The orientation is given in terms of the angle the long axis of a microfibril makes with the horizontal plane of the confocal image. From this the two dimensional nematic order parameter could be calculated as described in the manuscript text.

### S.I.5 Confocal Microscopy images of BC/CMC suspensions

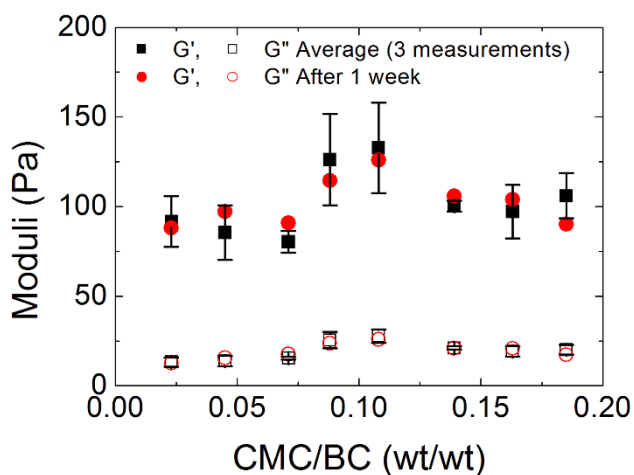
Confocal scanning laser microscopy (CSLM) was performed on a Leica TCS-SP5 confocal microscope. For staining,  $\sim 10 \mu\text{L}$  of 0.5 w/v % congo red solution in water was added to 1 mL of dispersion. For imaging, the samples were placed between two cover slips separated by a (3 mm) spacer. In the figure below images are shown from the BC dispersions at different CMC/BC ratios at a total BC volume fraction of  $\phi \sim 5 \times 10^{-3}$  (0.8 wt%, top row) as well as  $\phi \sim 1 \times 10^{-3}$  (0.2 wt%, bottom row).



**Supporting Figure 4:** From a (f) to e (j) the CMC/BC ratio increases from 0, 1/16 to 1/8, 3/16 and 1/4. Scale bar = 75  $\mu\text{m}$ . Top row: BC =  $\phi \sim 5 \times 10^{-3}$ , 0.8 wt%, Bottom row: BC =  $\phi \sim 1 \times 10^{-3}$ , 0.2 wt%.

### S.I.6 Change of moduli in time

Since bacterial cellulose is naturally attractive, the change in time of the moduli as shown in the manuscript may be due to a gradual increase in contacts between the particles. When this type of measurement was performed on the same suspension after a week of aging in the sample container no significant changes in the  $G'$  and  $G''$  after 5 minutes of oscillatory shear were seen (as compared to the average and determined error in the moduli of three individual measurements of the same sample performed a week earlier). The results of these measurements are shown in Supporting Figure 5. This leads us to believe that contacts between particles were initially destroyed by the force exerted onto the suspension by the lowering of the top plate in the rheometer and the gradual change in moduli may be due to the reformation of these contacts.



**Supporting Figure 5:** The elastic ( $G'$ ) and loss ( $G''$ ) modulus for CMC/BC suspensions with a BC volume fraction of  $\sim 2 \times 10^{-3}$  ( $\sim 0.4$  wt%). The average of three individual measurements was taken and compared to  $G'$  and  $G''$  as measured after 3 weeks of storage. Error bars are two times standard deviation.

### S.I.7 Full fit moduli fit results

The following table shows the fit results for a power-law fit of the suspension moduli as function of BC concentration (in volume fraction).

**Table 2:** Exponents of power-law fits

CMC/BC wt/wt	Standard deviation	Power-law fit $G'$			Power-law fit $G'' - \eta_s \omega$		
		Power n	Standard deviation	$R^2$	Power n	Standard deviation	$R^2$
0	0.00	3.53	0.06	0.998	3.31	0.08	0.996
0.023	0.009	3.16	0.10	0.995	2.94	0.12	0.990
0.045	0.009	3.12	0.06	0.998	2.90	0.07	0.996
0.071	0.009	3.22	0.09	0.996	2.96	0.05	0.999
0.088	0.009	3.03	0.10	0.994	2.82	0.07	0.996
0.108	0.009	3.15	0.12	0.991	2.91	0.07	0.996
0.139	0.011	3.20	0.08	0.996	2.88	0.06	0.997
0.163	0.009	3.24	0.16	0.985	2.83	0.08	0.995
0.185	0.010	3.22	0.09	0.996	2.80	0.11	0.991

### S.I.8 Void volume fraction determination and normalization

#### Void Volume fraction determination

To make an estimate of the void volume fraction ( $\xi_v$ ) in the CMC/BC networks, z-stacks were recorded in which confocal images of the network were taken at the same position but at different

depths. This was done at 40x magnification, resulting in a voxel dimension of (x,y,z) 378.8 nm by 378.8 n by 839.2 nm.

A 3D reconstruction of the network was made with ImageJ which was converted to a binary representation using the default settings of the “make binary” option. Since the pixel intensity histograms of the confocal images do not show a clear separation of the background and microfibril signals (it consists of a single yet asymmetric peak) an automatic thresholding algorithm was used. The default “make binary” option uses automatic thresholding by means of an Isodata algorithm and an iterative technique to split the pixel intensity histogram into two parts, each with a distinct intensity average to determine the threshold value.<sup>6</sup> The histogram is initially segmented into two parts using a starting threshold value ( $\theta_0$ ) for instance at half the maximum dynamic range (gray values found in the image). Then the sample mean of the gray values associated with the foreground pixels ( $m_{f,0}$ ) and the sample mean of the gray values associated with the background pixels ( $m_{b,0}$ ) are calculated. A new threshold value  $\theta_1$  is determined by taking the average of the two sample means. The process is then repeated but now based upon the new threshold until the threshold values doesn't change:

$$\theta_k = (m_{f,k-1} + m_{b,k-1})/2 \quad \text{Until } \theta_k = \theta_{k-1}$$

In this way a representation is obtained in which regions with a high microfibril density are converted into white voxels, while the background (containing no to very low microfibril concentrations) is converted to black voxels.  $\xi_v$  was set equal to the fraction of black voxels. Other automatic thresholding schemes were also used, for instance Huang<sup>7</sup>, Li<sup>8</sup>, Maximum Entropy<sup>9</sup>, Mean<sup>10</sup>, Otsu<sup>11</sup> and other methods. Each of them determines a threshold value in a different manner. For instance, by minimizing the fuzziness or the cross entropy of the background and microfibril part of the image. Or maximizing the entropy of the sum of the background and microfibril part, or using the variance of the two parts as an optimization criteria. Using the different threshold determination methods however, did not change the resulting binary images and the same value for the void volume fraction was found in all cases as can be seen in Table 3 below for selected BC concentrations and CMC/BC ratios.

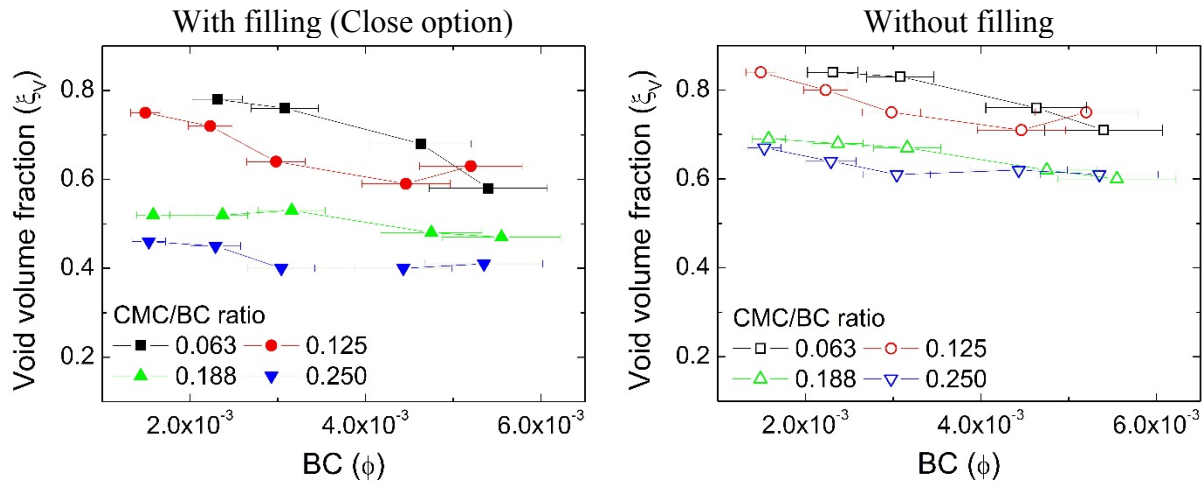
The network part of the system also contained some degree of holes but significantly smaller than the void size. Using the “Close” operation in ImageJ the part of the system containing fibrils can be smoothed and smaller holes can be filled. This operation performs a dilation followed by an erosion step, meaning that first pixels are added to the edge of objects after which a layer of pixels is again removed from the edge of objects. In each step, the full 3x3 environment of the object edge pixel is evaluated; hence, both neighboring pixels sharing a side as well as neighboring pixels sharing a corner are taken into account. Applying this smoothing step gives a better indication of the actual  $\xi_v$  of the system. The graphs shown in Supporting Figure 6 show the effect of this operation on the determined void volume fraction. As can be seen, the trend with respect to microfibril concentration (BC) and CMC/BC ratio does not alter. For high CMC/BC ratios there is no dependence of  $\xi_v$  on BC concentration, while for low ratios  $\xi_v$  decreases slightly. The Close operation does affect the absolute values for  $\xi_v$ .

The data represented in the paper was obtained using the Isodata algorithm in combination with the Close operation.

**Table 3:** Void volume fraction as determined from 3D binary images by using different intensity histogram thresholding methods for two CMC/BC ratios and two BC volume fractions.

CMC/BC ratio (wt/wt)	BC Volume frac.	Method	Void Volume frac.	CMC/BC ratio (wt/wt)	BC Volume frac.	Method	Void Volume frac.
0.063	1.54E-03	Isodata	0.82	0.063	4.63E-03	Isodata	0.77
0.063	1.54E-03	Huang	0.82	0.063	4.63E-03	Huang	0.77
0.063	1.54E-03	Li	0.82	0.063	4.63E-03	Li	0.77
0.063	1.54E-03	MaxEntropy	0.82	0.063	4.63E-03	MaxEntropy	0.77
0.063	1.54E-03	Mean	0.82	0.063	4.63E-03	Mean	0.77
0.063	1.54E-03	Otsu	0.82	0.063	4.63E-03	Otsu	0.77

CMC/BC ratio (wt/wt)	BC Volume frac.	Method	Void Volume frac.
0.250	4.43E-03	Isodata	0.66
0.250	4.43E-03	Huang	0.66
0.250	4.43E-03	Li	0.66
0.250	4.43E-03	MaxEntropy	0.66
0.250	4.43E-03	Mean	0.66
0.250	4.43E-03	Otsu	0.66



**Supporting Figure 6:** Void volume fraction as determined from 3D binary images both with and without including the Close operation step which smooths edges and fills up holes.

## Normalization of elastic moduli

The analysis splits the system onto two parts: a network part containing fibrils and a void part without fibrils. Due to the presence of voids, the concentration of fibrils in the network part ( $\phi_N$ ) is higher than the overall fibril concentration ( $\phi$ ).  $\phi_N$  can easily be calculated by means of  $\phi_N = \phi/(1 - \xi_V)$ .

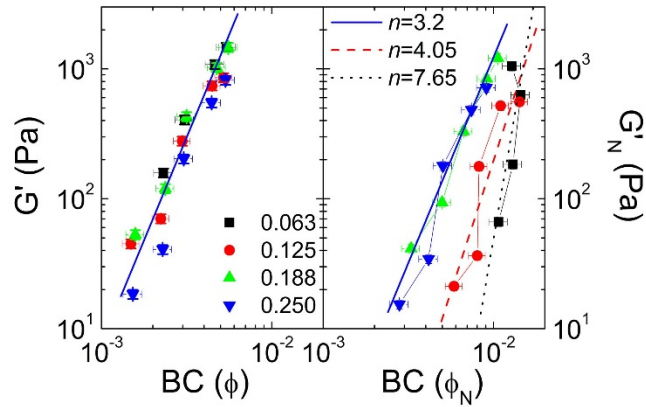
In order to calculate the elastic modulus of the network part, a so called Reuss-Voigt-Hill averaging scheme (RVH) is used. The RVH averaging scheme is a mean of the Voigt and Reuss bounds and is frequently used in material science to predict several different properties of composite materials containing fiber-like constituents. The Voigt and Reuss bounds themselves assume that the fibers are all aligned and give expressions for properties as the elastic modulus when either axial or transverse loading is applied. This is done by using a weighted mean of the properties of the different parts of the composite.<sup>12,13</sup> These simple descriptions and their mean have been used to describe and/or predict material properties as the elastic modulus and percolation threshold for, in particular, cellulose fibrils and rod-like whisker containing materials and dispersions.<sup>15-18</sup> It has also been used in a simple model for characterization of non-uniform fiber-based composites and networks.<sup>14</sup>

The Voigt ( $G'_{Voigt}$ ) and Reuss ( $G'_{Reuss}$ ) bounds are defined as followed.

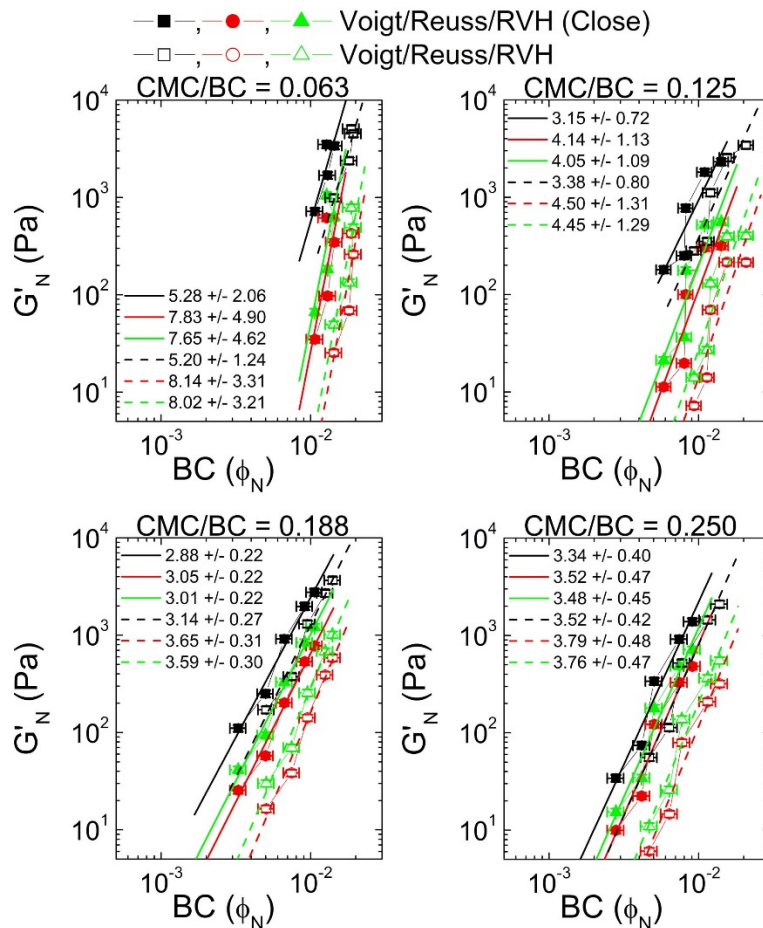
$$G'_{Voigt} = \sum_{i=1}^N \xi_i G'_i \quad \text{and} \quad G'_{Reuss} = \left( \sum_{i=1}^N \xi_i G'_i \right)^{-1}$$

Here  $\xi_i$  and  $G'_i$  are the fraction of the total volume and value of the elastic modulus of constituent  $i$  of the composite. The RVH scheme is the arithmetic mean of the two given bounds, namely  $G' = (G'_{Voigt} + G'_{Reuss})/2$ . If the CMC/BC system can indeed be seen as consisting of two parts (voids and network), then the overall  $G'$  is a combination of the modulus of the network ( $G'_N$ ) and that of the voids ( $G'_V$ ). Since the voids essentially contain no fibrils it also does not have a modulus, while  $G'_N$  still depends on  $\phi_N$ .

The results for the normalization of the network elastic modulus by means of the RVH averaging scheme are shown in Supporting Figure 7. This data is also presented in the paper. Here the power-law behavior of the overall elastic moduli ( $G'$ ) as a function of the overall BC volume fraction ( $\phi$ ) is compared to the BC volume fraction ( $\phi_N$ ) and elastic modulus ( $G'_N$ ) of only the network part. For the two lowest ratios, the power-law behavior changes to a high exponent of 7.65 at CMC/BC 0.063 and 4.05 at CMC/BC 0.125. After reaching a ratio of 0.188 the power-law again has an exponent of  $\sim 3.2$  as was seen for the overall elastic modulus. For CMC/BC ratios of 0.188 and 0.125 the dependence only shifts without changing the exponent. Accounting for the presence of voids the exponent in the power-law now decreases with the increase in alignment and homogeneity of the microstructure as a result of the increase in CMC concentration. This finding is a direct evidence for changes in the interactions between the fibrils in the macroscopically homogeneous regions (i.e. without voids) when charged adsorbing polymer is added.



**Supporting Figure 7:** Comparison of power-law behavior before and after normalization for the void volume fraction.



**Supporting Figure 8:** Elastic modulus ( $G'$ ) as a function of bacterial cellulose (BC) microfibril volume fraction for four different CMC/BC ratios. Different symbols represent data points obtained from different void volume fraction determinations and different averaging schemes for the moduli. Lines represent power-law fits of with the exponent  $n$  is given in the inset.

The RVH mean has been proven to work well for random distributions of the fibrils.<sup>12,13</sup> In our systems, however, the distribution of the micro-fibrils is not always random (for example in the

nematic-type areas). It is therefore useful to consider the effect of the limiting behaviors with respect to elastic modulus averaging. The effect of the RVH averaging scheme and the Voigt and Reuss bounds on the absolute values and power-law behavior of the elastic modulus for four different CMC/BC ratios is given in Supporting Figure 8. Data is presented for determination of the void volume fraction with and without smoothing in the form of the Close procedure. As can be seen, when the same procedure is used for all ratios, the trend in power-law change remains similar: decreasing exponent with increasing CMC/BC ratio. The absolute values for the elastic moduli, however, can change significantly (up to an order of magnitude) depending on which averaging scheme is used for the determination of the  $G'$  of the network part of the system.

- 1 T. G. Mezger, *The Rheology Handbook*, Vincentz Network, Hanover, Third rev., 2011.
- 2 H. A. Barnes, *A handbook of elementary rheology*, University of Wales, Wales, 2000.
- 3 A. Villay, F. Lakkis de Filippis, L. Picton, D. Le Cerf, C. Vial and P. Michaud, *Food Hydrocoll.*, 2012, **27**, 278–286.
- 4 S. J. Veen, A. Kuijk, P. Versluis, H. Husken and K. P. Velikov, *Langmuir*, 2014, **30**, 13362–13368.
- 5 R. Rezakhaniha, A. Agianniotis, J. T. C. Schrauwen, A. Griffa, D. Sage, C. V. C. Bouten, F. N. van de Vosse, M. Unser and N. Stergiopoulos, *Biomech. Model. Mechanobiol.*, 2012, **11**, 461–473.
- 6 T. W. Ridler and S. Calvard, *IEE Trans. Syst. man, Cybern.*, 1978, **SMC-8**, 630–632.
- 7 L. K. Huang and M. J. J. Wang, *Pattern Recognit.*, 1995, **28**, 41–51.
- 8 C. H. Li and P. K. S. Tam, *Pattern Recognit. Lett.*, 1998, **19**, 771–776.
- 9 J. N. Kapur, P. K. Sahoo and a. K. C. Wong, *Comput. Vision, Graph. Image Process.*, 1985, **29**, 140.
- 10 C. A. Glasbey, *CVGIP Graph. Model. image Process.*, 1993, **55**, 532–537.
- 11 N. Otsu, *IEEE Trans. Syst. Man. Cybern.*, 1979, **smc-9**, 62–66.
- 12 A. Reuss, *Zeitschrift für Angew. Math. und Mech.*, 1929, **9**, 49–58.
- 13 W. Voigt, *Ann. Phys.*, 1889, **274**, 573–587.
- 14 A. P. Chatterjee, *J. Phys. Condens. Matter*, 2011, **23**, 155104.
- 15 M. A. S. A. Samir, F. Alloin and A. Dufresne, *Biomacromolecules*, 2005, **6**, 612–626.
- 16 V. Favier, R. Dendievel, G. Canova, J. Y. Cavaille and P. Gilormini, *Acta Mater.*, 1997, **45**, 1557–1565.

- 17 R. J. Hill, *Biomacromolecules*, 2008, **9**, 2963–2966.
- 18 A. P. Chatterjee, *J. Appl. Phys.*, 2010, **108**.